OPEN ACCESS Freely available online

PLOS ONE

Baseline Monitoring of the Western Arctic Ocean Estimates 20% of Canadian Basin Surface Waters Are Undersaturated with Respect to Aragonite

Lisa L. Robbins[1]*, Jonathan G. Wynn[2], John T. Lisle[1], Kimberly K. Yates[1], Paul O. Knorr[1], Robert H. Byrne[3], Xuewu Liu[3], Mark C. Patsavas[3], Kumiko Azetsu-Scott[4], Taro Takahashi[5]

1 St. Petersburg Coastal and Marine Science Center, United States Geological Survey, St. Petersburg, Florida, United States of America, **2** Department of Geology, University of South Florida, Tampa, Florida, United States of America, **3** College of Marine Science, University of South Florida, St. Petersburg, Florida, United States of America, **4** Ocean Sciences Division, Department of Fisheries and Oceans, Bedford Institute of Oceanography, Dartmouth, Nova Scotia, Canada, **5** Lamont-Doherty Earth Observatory of Columbia University, Palisades, New York, United States of America

Abstract

Marine surface waters are being acidified due to uptake of anthropogenic carbon dioxide, resulting in surface ocean areas of undersaturation with respect to carbonate minerals, including aragonite. In the Arctic Ocean, acidification is expected to occur at an accelerated rate with respect to the global oceans, but a paucity of baseline data has limited our understanding of the extent of Arctic undersaturation and of regional variations in rates and causes. The lack of data has also hindered refinement of models aimed at projecting future trends of ocean acidification. Here, based on more than 34,000 data records collected in 2010 and 2011, we establish a baseline of inorganic carbon data (*p*H, total alkalinity, dissolved inorganic carbon, partial pressure of carbon dioxide, and aragonite saturation index) for the western Arctic Ocean. This data set documents aragonite undersaturation in ~20% of the surface waters of the combined Canada and Makarov basins, an area characterized by recent acceleration of sea ice loss. Conservative tracer studies using stable oxygen isotopic data from 307 sites show that while the entire surface of this area receives abundant freshwater from meteoric sources, freshwater from sea ice melt is most closely linked to the areas of carbonate mineral undersaturation. These data link the Arctic Ocean's largest area of aragonite undersaturation to sea ice melt and atmospheric CO_2 absorption in areas of low buffering capacity. Some relatively supersaturated areas can be linked to localized biological activity. Collectively, these observations can be used to project trends of ocean acidification in higher latitude marine surface waters where inorganic carbon chemistry is largely influenced by sea ice meltwater.

Citation: Robbins LL, Wynn JG, Lisle JT, Yates KK, Knorr PO, et al. (2013) Baseline Monitoring of the Western Arctic Ocean Estimates 20% of Canadian Basin Surface Waters Are Undersaturated with Respect to Aragonite. PLoS ONE 8(9): e73796. doi:10.1371/journal.pone.0073796

Editor: Rodolfo Paranhos, Instituto de Biologia, Brazil

Received February 26, 2013; **Accepted** July 25, 2013; **Published** September 11, 2013

Funding: The study was funded by U.S. Geological Survey Coastal and Marine Program and U.S. Geological Survey's Office of the Regional Executive- Alaska to LLR. Ship time for the ECS cruises was funded by NOAA grant NA10NOS4000073. Additional support came from NSF grant ARC-1220032 to JGW and LLR, NOAA Ocean Acidification Program to RHB and the Office of Climate Observation of NOAA to TT. The funders had no role in study design, data collection and analysis, decision to publish, or preparation of the manuscript.

Competing Interests: The authors have declared that no competing interests exist.

* E-mail: lrobbins@usgs.gov

Introduction

The importance of the Arctic Ocean in the context of global carbon dioxide (CO_2) uptake and ocean acidification is widely accepted [1–9]. Ocean acidification is projected to occur relatively rapidly in the Arctic due to processes and conditions that are unique to Arctic surface waters [7–9]. For instance, a large fraction of the global net CO_2 uptake during recent decades (~2200 Tg C yr^{-1}) has occurred over the relatively small surface area of the Arctic Ocean. From the estimated net CO_2 uptake rates of the Arctic Ocean (65–175 Tg C yr^{-1}; reviewed in ref. [8]), it is inferred that as much as 7.5% of global oceanic CO_2 uptake may occur in the Arctic Ocean, which comprises only 3.9% of the global ocean's surface. These figures may be even more noteworthy given that the uptake occurs predominantly in seasonally ice-free areas, which are a fraction of the Arctic Ocean surface.

One driving factor behind the disproportionate Arctic Ocean CO_2 uptake and resulting acidification is the relatively cold surface water, which absorbs more CO_2 than warmer seawater [3,5]. Furthermore, over the past decade, summer sea ice extent has rapidly declined [9–13], reaching a record low in 2012 [14]. Multiyear sea ice has experienced the greatest decline [9]. This loss of multiyear ice has exposed the surface mixed layer (typically≤50 m thick), which is undersaturated with respect to atmospheric CO_2; the result is oceanic CO_2 uptake. Previously, ice cover significantly inhibited CO_2 exchange between this layer and the atmosphere [15–17].

This melt-associated exposure of undersaturated waters is unique to the Arctic, where a steep vertical density gradient, attributable primarily to a cold halocline underlying the surface mixed layer, inhibits upward mixing of CO_2-rich deep waters, even during winter when the mixed layer temperature is lowest and salinity is highest due to sea ice formation [18]. Unlike the Southern Ocean seasonal ice zone, where the under-ice water has

a relatively high partial pressure of CO_2 (pCO_2~420 µatm) due to rapid vertical mixing of Circumpolar Deep Water [19], the mixed layer immediately under Arctic sea ice remains low in salinity and pCO_2. Thus, when Arctic sea ice melts in summer, the under-ice layer is exposed to the atmosphere and is also diluted by freshwater from sea ice melt. This dilution is an important consequence of multiyear sea ice loss because it reduces surface seawater calcium and carbonate ion concentrations and pH [20,21]. The combination of these processes is expected to drive the expansion of areas of carbonate mineral undersaturation in the Arctic Ocean over the next decades [3–6].

The in situ melting of sea ice has a number of direct consequences for seawater chemistry. The saturation state index of carbonate minerals (Ω_{carb}) is defined by:

$$\Omega_{carb} = \left[Ca^{2+}\right]\left[CO_3^{2-}\right]/K_{sp}$$

where [Ca^{2+}] is the calcium ion concentration, [CO_3^{2-}] is the

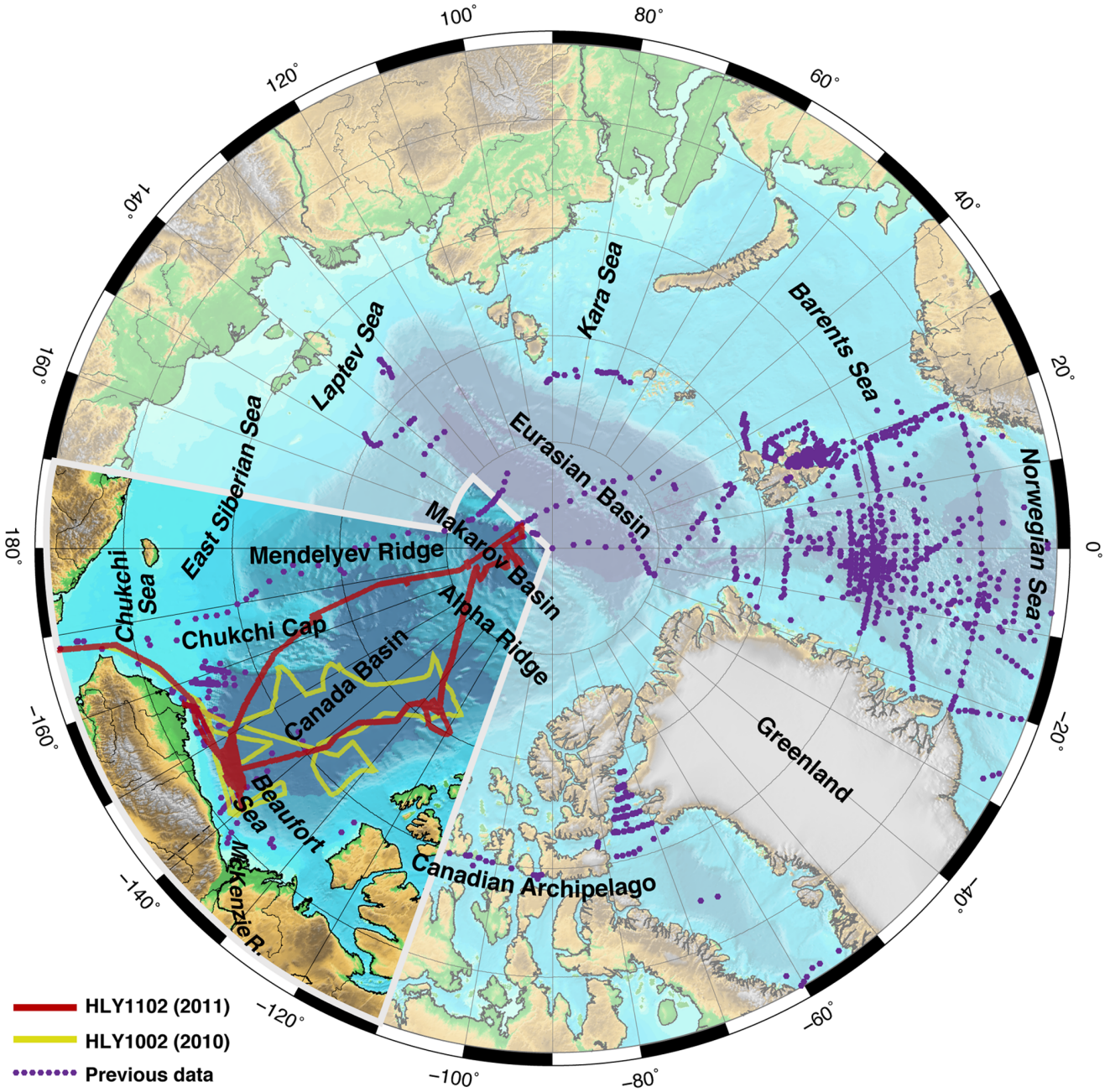

Figure 1. Location map of Arctic Ocean underway and discrete inorganic carbon data. Locations are shown for the HLY1002 and HLY1102 cruises, as well as previous work. Previous data are from the Carbon Dioxide Information Analysis Center (http://cdiac.ornl.gov/oceans/datmet.html), Japan Agency for Marine Earth Science and Technology (http://www.godac.jamstec.go.jp/dataportal/viewer.htm), and BioChem (http://www.meds-sdmm.dfo-mpo.gc.ca/BioChem/biochem-eng.htm). Digital bathymetry is from the International Bathymetric Chart of the Arctic Ocean [48]. The highlighted sector is shown in subsequent figures.
doi:10.1371/journal.pone.0073796.g001

carbonate ion concentration, and K_{sp} is the stoichiometric solubility product of the mineral. This index provides a quantitative measure of the thermodynamic potential for carbonate minerals such as aragonite and calcite to either precipitate ($\Omega_{carb}>1$) or dissolve ($\Omega_{carb}<1$). Importantly, when multiyear sea ice melts, fresh water containing relatively little carbonate and calcium is liberated, thereby lowering Ω_{carb} of the receiving seawater. The resulting changes in pH, Ω_{carb}, and pCO_2 affect calcifying organisms at the base of the food chain, creating effects that propagate through higher trophic levels [1,3]. Thus, the expansion of acidification into areas previously isolated from atmospheric contact by multiyear ice cover is likely to have ecological and economic consequences.

Ocean acidification models project that under a number of plausible scenarios of increasing atmospheric CO_2, the Arctic Ocean will become undersaturated with respect to carbonate minerals in the next decade [3–6]. Recent data indicate that some areas are already undersaturated with respect to the carbonate mineral aragonite [16,21–25]. These areas, which include regions of the Canadian Archipelago, Canada Basin, and Beaufort Sea, exhibit the lowest aragonite saturation state (Ω_a) values during late summer, when sea ice is at its minimum annual extent. However, the spatial extent of undersaturated waters in the western Arctic Ocean has been poorly constrained.

Much of the uncertainty of models that project future trends of Arctic Ocean acidification is due to inadequate data coverage, particularly in higher latitudes. As of late 2011, only ~20,000 data points were available in public databases for the entire Arctic Ocean (surface and water column; data from refs. [16,17,21–26] and the data sets of the Japan Agency for Marine Earth Science and Technology, BioChem, and the Carbon Dioxide Information Analysis Center, including CARINA and GLODAP; Figure 1). Most of the data are from the Atlantic/Norwegian Sea (Figure 1). Establishing carbonate chemistry baselines and improving our understanding of the processes that drive changes in carbonate chemistry are fundamental for constraining the biogeochemical process parameters needed to predict ocean acidification effects on Arctic Ocean flora and fauna. Thus, a systematic approach for measuring the carbonate chemistry of the Arctic Ocean at high spatial resolution from coastal to pelagic waters is needed.

To begin to establish these baselines and fill critical data gaps, we collected carbonate chemistry data at high spatial resolution in the western Arctic Ocean during 2010 and 2011. We supplemented these data with measurements of conservative tracers of water sources as well as proxies of biological processes. This study compares aragonite saturation states in open pelagic waters, shallow shelf waters, and ice-bound high-latitude waters to delineate rates of change and causes of variation in carbonate mineral saturation states.

Materials and Methods

From 3 August to 5 September 2010 and from 16 August to 28 September 2011, we collected seawater chemical and biological measurements as noninterference science on United States (U.S.) Extended Continental Shelf Task Force cruises aboard the U.S. Coast Guard Cutter *Healy* in the western Arctic Ocean (Figure 1). No specific permissions were required for collecting water samples in Arctic international waters or U.S. or Canadian waters. Our studies did not involve endangered or protected species. Continuous and discrete water samples (Table 1) were collected underway from ~8 m below the waterline, via a port in the ship's hull. Approximately 25,000 data records resulted from the 2010 cruise; approximately 9,000 data records resulted from the 2011 cruise.

Underway Continuous Measurements

Geographic position, salinity (S), temperature (T), and fluorometric data ($n = 62,387$) were collected using a shipboard Ashtech ADU5 GPS system, a SeaBird SBE45 thermosalinograph, and a Seapoint Chlorophyll Fluorometer [27]. The majority of the carbonate chemical measurements were made using a Multiparameter Inorganic Carbon Analyzer (MICA) [28], a flowthrough system which measured pH, pCO_2, and total dissolved inorganic carbon (TCO_2), along with S and T ($n = 34,000$). Data were logged approximately every 2 mins on the 2010 cruise and every 7 mins on the 2011 cruise. The MICA was calibrated using Certified Reference Material from Professor A. Dickson of the University of California at San Diego. Precision was ± 0.002 for pH, ± 2 µatm for pCO_2, and ± 2 µmol kg^{-1} for TCO_2. A Lamont-Doherty Earth Observatory underway system for surface water measurements was also used to measure pCO_2 during the 2011 cruise ($n = 18,500$). This system was calibrated every 4 hrs using five calibration gas mixtures certified by the National Oceanic and Atmospheric Administration (NOAA) Climate Monitoring and Diagnostic Laboratory. The precision of the pCO_2 seawater values is about ± 1.5 µatm.

Discrete Surface Samples and Analyses

Discrete surface water samples were collected from the underway system every 1–4 hrs following the protocols of ref. [29]. The samples ($n \cong 560$) were immediately analyzed for pH using purified meta-cresol purple indicator dye and the method and equations of ref. [30].

Table 1. Methods used to measure carbonate system parameters on the HLY1002 (2010) and HLY1102 (2011) cruises.

Sample Type	Analysis	Parameter	Approx. sample interval (year)
Continuous (flow-through)	USF Multiparameter Inorganic Carbon Analyzer (MICA) – spectrophotometric – on ship	pH, pCO_2, TCO_2	2 min (2010); 7 min (2011)
Continuous (flow-through)	LDEO Underway system for surface water pCO_2– infrared gas analyzer – on ship	pCO_2	3 min (2011)
Discrete (optical cell)	Spectrophotometric – on ship	pH	1–4 hr (2010); 1 hr (2011)
Discrete (bottle)	Coulometric, titrimetric – land-based lab	TCO_2, TA	8 hr (2010); 1–4 hr (2011)
Discrete (bottle)	Isotope ratio mass spectrometry – land-based lab	$\delta^{18}O$	8 hr (2010); 1–4 hr (2011)

doi:10.1371/journal.pone.0073796.t001

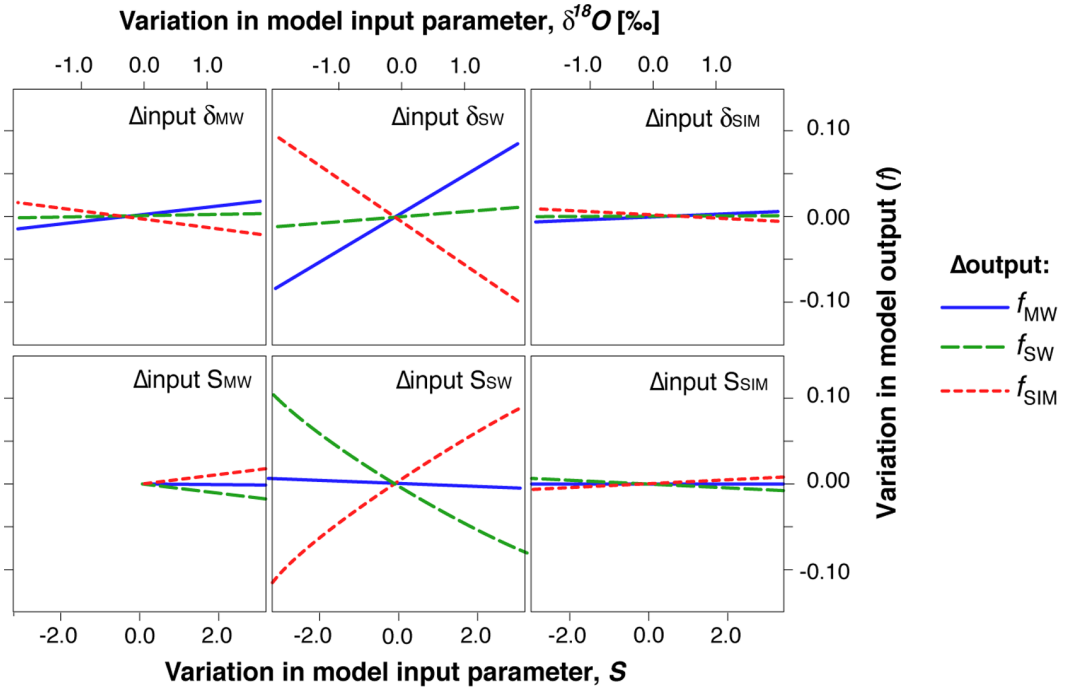

Figure 2. Sensitivity of mixing-model output (f_{SW}, f_{SIM}, and f_{MW}) to variations in assumed end-member compositions. Upper panels show the effect of varying end-member $\delta^{18}O$ by 10% of the observed $\delta^{18}O$ range: i.e., by $\pm 0.1(\delta^{18}O_{max} - \delta^{18}O_{min}) = \pm 0.2‰$. Lower panels show the effect of varying end-member S by 10% of the observed S range: i.e., by $\pm 0.1(S_{max} - S_{min})$. Model sensitivity is calculated for a hypothetical sample with S and $\delta^{18}O$ equal to the mid-range values of the combined HLY1002 and HLY1102 data sets: $S_{model} = S_{min} + ½(\text{range } S)$ and $\delta^{18}O_{model} = \delta^{18}O_{min} + ½(\text{range } \delta^{18}O)$.
doi:10.1371/journal.pone.0073796.g002

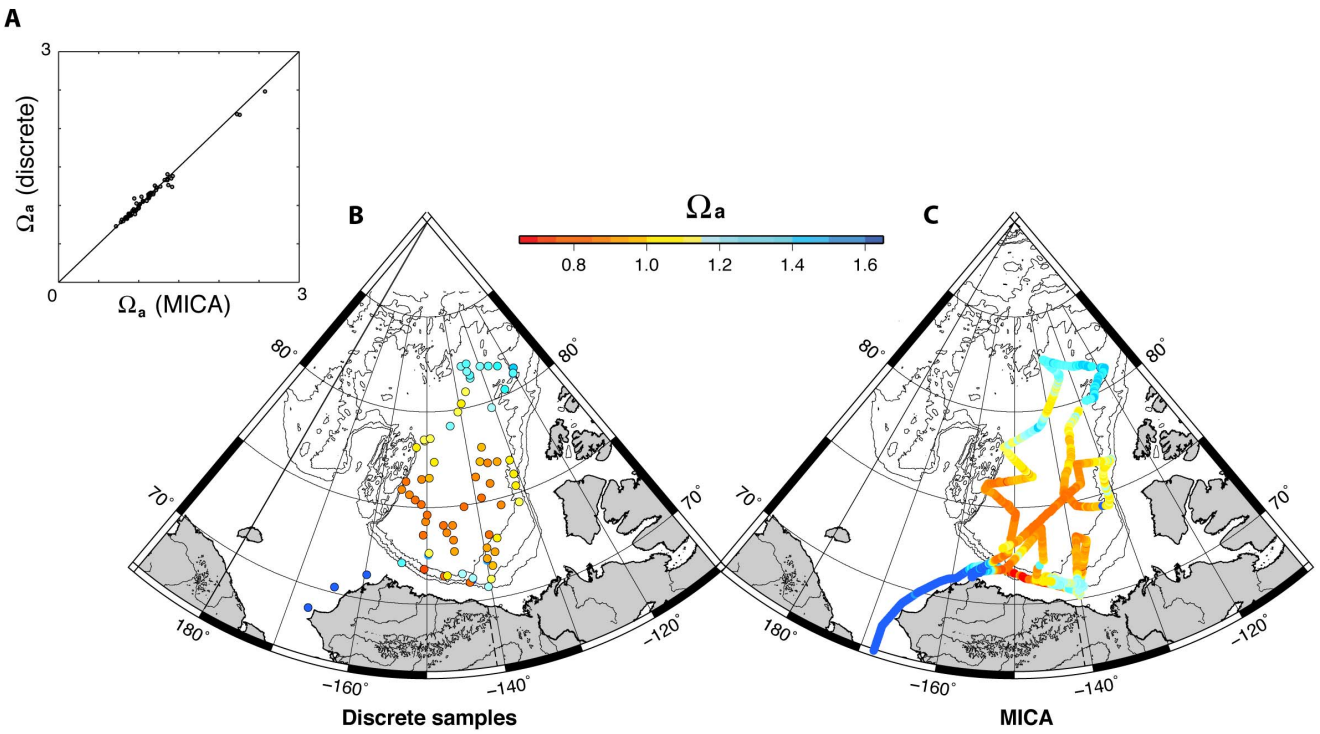

Figure 3. Aragonite saturation state, Ω_a, calculated from discrete samples and from underway MICA readings. (A) Cross plot of discrete sample values with nearest-neighbor MICA values. (B) Map of 2010 discrete sample values. (C) Map of 2010 MICA values.
doi:10.1371/journal.pone.0073796.g003

Table 2. Regional median values (and ranges) for 2011 surface water data and mixing-model output.

Parameter (units)	Beaufort Sea	Makarov Basin	Sever Spur	Canada Basin
	(*n* = 53)	(*n* = 49)	(*n* = 24)	(*n* = 103)
Ω_a	1.15 (0.85–1.35)	1.52 (1.25–1.61)	1.25 (1.14–1.46)	1.04 (0.70–1.84)
f_{SIM}	0.083 (–0.009–0.215)	−0.010 (–0.035–0.027)	0.041 (0.016–0.061)	0.080 (−0.024–0.219)
f_{MW}	0.252 (0.170–0.307)	0.137 (0.116–0.119)	0.151 (0.132–0.177)	0.171 (0.054–0.256)
f_{Sw}	0.664 (0.553–0.816)	0.877 (0.825–0.900)	0.805 (0.786–0.840)	0.742 (0.525–0.932)
T (°C)	5.91 (2.22–7.96)	–1.63 (−1.68– −1.49)	–1.50 (−1.58– −1.48)	−1.32 (−1.54−7.99)
S	23.51 (19.11–28.47)	30.61 (28.75–31.35)	28.28 (27.69–29.43)	26.25 (19.22–32.60)
pCO_2 (µatm)	370.3 (310.6–386.1)	264.0 (242.7–330.4)	335.3 (331.9–338.5)	322.9 (247.4–554.9)
*p*H	8.05 (8.03–8.13)	8.19 (8.13–8.22)	8.15 (8.10–8.21)	8.07 (7.76–8.20)
Chl-a ($\mu g \cdot L^{-1}$)	0.19 (0.11–0.31)	0.29 (0.19–0.46)	0.22 (0.20–0.26)	0.17 (0.09–1.86)
BP (mg $C \cdot L^{-1} \cdot d^{-1}$)	3.27 (1.37–4.34)	0.62 (0.53–0.69)	0.59 (0.58–0.61)	0.53 (0.004–4.48)

doi:10.1371/journal.pone.0073796.t002

Additional discrete samples were collected every 1–8 hrs for post-cruise laboratory analysis of *TA* and TCO_2 ($n \cong 305$) as well as oxygen isotopic composition ($n \cong 307$). *TA* was measured spectrophotometrically and TCO_2 was measured coulometrically, both following the procedures of ref. [29], at the Carbon Analysis Laboratory of the U.S. Geological Survey (USGS) St. Petersburg Coastal and Marine Science Center. Stable oxygen isotopic analyses were completed at the University of South Florida Department of Geology's Stable Isotope Laboratory with a Thermo-Finnigan Delta V 3 keV Isotope Ratio Mass Spectrometer coupled to a Gasbench II preparation device. Stable isotopic data are expressed in the conventional delta (δ) notation: $\delta^{18}O = [(^{18}O/^{16}O_{sample} - {}^{18}O/^{16}O_{standard})/(^{18}O/^{16}O_{standard})]$ where δ is expressed in per mil (‰) with respect to the VSMOW standard scale. Analytical precision (2σ) on these standards was better than 0.15‰ and 0.10‰ for $\delta^{18}O$ from HLY1002 and HLY1102, respectively.

Water Mass Mixing Model

To identify sources of water masses, we applied a three-component mixing model based on measurements of salinity (*S*) and oxygen isotopic composition ($\delta^{18}O$). This mixing model is well suited to quantify fractional contributions (*f*) from various sources–in this case, meteoric fresh water and sea ice meltwater mixing with seawater. Meteoric freshwater (MW), derived from terrestrial runoff and direct precipitation, has negligible salinity ($S \cong 0$) but is relatively ^{18}O-depleted in the high latitudes of the Arctic ($\delta^{18}O \cong$ –20‰). Sea ice melt (SIM) also has relatively low salinity ($S < 5$), but its oxygen isotopic composition is similar to that of seawater, from which it is formed ($\delta^{18}O \cong 0$ to –6‰). Seawater (SW) has salinity of 32–35 and $\delta^{18}O$ values of –1 to +0.3‰, although these values vary between Atlantic and Pacific source regions. This freshwater tracer method, which takes advantage of the large differences in the $\delta^{18}O$ values of the freshwater sources [31], has been used for decades to partition surface waters into constituent water sources [32–38].

Using discrete measurements of *S* and $\delta^{18}O$, each surface water sample can be partitioned into a mixture of the three end-members, with the fractional contribution of each end-member determined by mass balance:

$$f_{MW} + f_{SIM} + f_{SW} = 1$$
$$f_{MW}(S_{MW}) + f_{SIM}(S_{SIM}) + f_{SW}(S_{SW}) = S_{measured}$$
$$f_{MW}(\delta_{MW}) + f_{SIM}(\delta_{SIM}) + f_{SW}(\delta_{SW}) = \delta_{measured}$$

where δ is shorthand notation for $\delta^{18}O$. We parameterize the model with estimates of *S* and $\delta^{18}O$ values (δ) of each of the three end-members. For the MW end-member, we use data from recent stream gauging studies, which provide an estimate of the flow-weighted $\delta^{18}O$ value from major Arctic rivers: $S_{MW} = 0$ and $\delta^{18}O_{MW} = -20 \pm 1$ ‰; [34,35,39]. Direct precipitation is estimated to have a similar $\delta^{18}O$ value. For the SIM end-member, we use salinity values of multiyear ice: $S_{SIM} = 4$ (ref. [40]). We calculate the $\delta^{18}O$ value of sea ice from the $\delta^{18}O$ value measured in the local

Table 3. Dunn's Method *Q*-statistic results for pairwise multiple comparisons of the four Arctic Ocean regions.

Pairwise Comparison	Ω_a	f_{SIM}	f_{MW}	f_{SW}	pCO_2	*T*	*S*	*Chl-a*	*BP*
Beaufort Sea vs. Makarov Basin	X	X	X	X	X	X	X	X	X
Beaufort Sea vs. Sever Spur	*ns*	X	X	X	X	X	X	*ns*	X
Beaufort Sea vs. Canada Basin	*ns*	*ns*	X	X	X	X	X	*ns*	X
Makarov Basin vs. Sever Spur	X	X	*ns*	X	X	*ns*	X	*ns*	*ns*
Makarov Basin vs. Canada Basin	X	X	X	X	X	X	X	X	X
Sever Spur vs. Canada Basin	X	X	*ns*	X	*ns*	X	X	X	*ns*

A significant difference ($p < 0.05$) between paired regions is denoted by an X, and a non-significant difference is denoted by *ns*. All comparisons were conducted at $\alpha = 0.05$.

doi:10.1371/journal.pone.0073796.t003

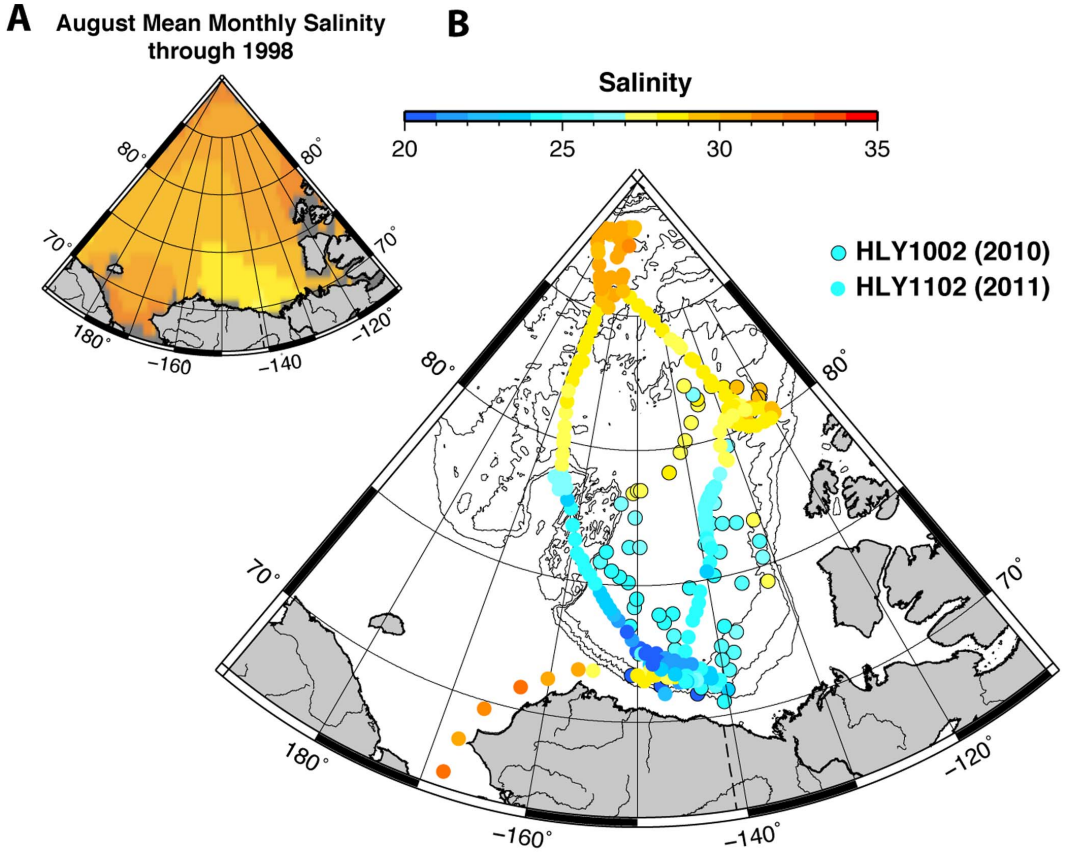

Figure 4. Surface salinity in the western Arctic Ocean. (A) Map showing August mean salinity (through 1997) at 10 m depth from the World Ocean Atlas 1998 [51]. Data provided by Physical Sciences Division, Earth System Research Laboratory, NOAA (http://www.esrl.noaa.gov/psd/). (B) Map of HLY1002 (2010) and HLY1102 (2011) discrete sample salinities.
doi:10.1371/journal.pone.0073796.g004

surface water plus a fractionation factor for liquid–solid water isotopic fractionation: $\delta^{18}O_{SIM} = \delta^{18}O_{measured} + 2.6‰$ [33,41]. Each cruise measurement of $\delta^{18}O$ therefore provides an individual estimate of $\delta^{18}O_{SIM}$. This approach, which differs somewhat from the static $\delta^{18}O_{SIM}$ approach used in some recent work [35,38], may be preferable in that a variable $\delta^{18}O_{SIM}$ value may take into account annual changes in the $\delta^{18}O$ values of both seawater and newly formed sea ice. For the SW end-member, we use estimates of the composition of the inflow from the Atlantic ($S_{SW} = 34.92 \pm 0.05$ and $\delta^{18}O_{SW} = 0.3 \pm 0.1$ ‰), although we recognize that Arctic seawater, particularly in the southern Canada Basin, is partially derived from Bering Strait Inflow (BSI), which typically has lower salinity and $\delta^{18}O$ values ($S_{BSI} = 32.5$ and $\delta^{18}O_{BSI} = -0.8 \pm 0.1$ ‰; ref. [38]) due to dilution by Bering Sea freshwater inputs. Previous studies have used a variety of characterizations for the seawater end-member in the western Arctic [32,38,42]. The advantage of using Atlantic inflow seawater rather than BSI seawater for SW end-member values is that we are then able to make comparisons with other pan-Arctic studies of water sources. The disadvantage is that our calculated f_{MW} values may be overestimates. In other words, our calculated f_{MW} values, attributed to Arctic river runoff and direct precipitation, may also reflect the influence of freshwater that derives from BSI. Adding dissolved silica measurements to the mass balance model could provide a means of independently quantifying the additional BSI source [34,38].

Figure 2 illustrates the sensitivity of estimated f values (mixing-model output) to uncertainties in end-member compositions. The mixing model is relatively insensitive to analytical errors, which are small (~0.01 and 0.1‰ for S and $\delta^{18}O$, respectively) relative to other sources of uncertainty. The model is most sensitive to potential systematic error introduced by incorrect assumptions regarding the SW end-member.

Aragonite Saturation States

In situ aragonite saturation states (Ω_a) were calculated using the CO2calc carbon calculator application [43]. Input parameters were the TA–pH data pair, carbonic acid dissociation constants (pK_1 and pK_2) from Lueker et al. [44], HSO_4^- dissociation constants from Dickson [45], and the borate dissociation constant of Lee et al. [46] and other measured parameters such as T, S. The solubility product (K_{sp}) for aragonite was derived from Mucci [47]. Internal consistency was established by comparing Ω_a derived using the TA–pH pair with Ω_a derived using the TCO_2–pH pair or TCO_2–pCO_2 pair. On the basis of these consistency test results, we estimate a precision of ±0.05 for Ω_a.

Values of Ω_a calculated from coincident MICA and discrete sample analyses (i.e., coincident TA–pH data pairs; $n = 68$) were statistically compared as an estimation of the equivalence of the two data sets. Spearman rank-order correlation shows the two data sets are highly and positively correlated ($R^2 = 0.985$; $p < 0.001$). The Mann-Whitney ($\alpha = 0.05$) test for significant differences ($W = 4712.0$; $p = 0.816$) found no significant difference between the two data sets. Based on this equivalence (Figure 3A), we use Ω_a values calculated from the discrete samples (Figure 3B) to compare

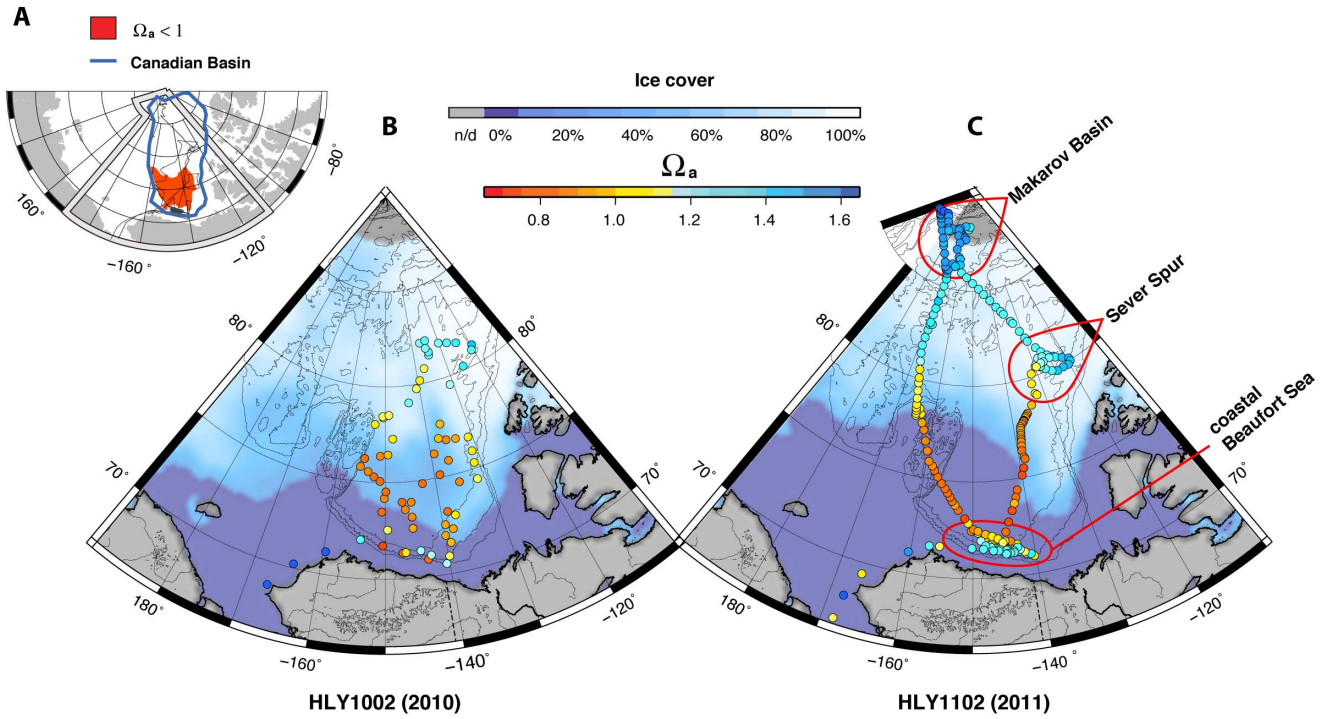

Figure 5. Surface water aragonite saturation state (Ω_a) and ice cover in the western Arctic Ocean. (A) Canadian Basin (outlined in blue) and area of surface Ω_a undersaturation during 2010–2011 (red). (B) HLY1002 aragonite saturation state. (C) HLY1102 aragonite saturation state. Maps (B) and (C) also show average sea ice concentration (% ice cover) for August 2010 and September 2011, respectively [70]. The Makarov Basin, Sever Spur, and coastal Beaufort Sea regions are encircled in red; the remaining data points are assigned to the Canada Basin region. All Ω_a values are calculated from discrete sample data.
doi:10.1371/journal.pone.0073796.g005

to other discrete sample measurements, and we use Ω_a values calculated from the MICA data (Figure 3C) to provide more detailed spatial resolution of Ω_a distributions.

The areal extent of aragonite undersaturation ($\Omega_a<1$) was estimated using ESRI ArcGIS software (version 10.1). Ω_a values calculated from the 2010 and 2011 cruises (>21,000 data points) were projected and then used to interpolate a raster map of aragonite undersaturation in the Makarov and Canada basins, both part of the Canadian Basin. A natural neighbor routine was used for the interpolation. The Makarov Basin (334,224 km^2) and Canada Basin (1,524,664 km^2) were delineated and measured by tracing the surrounding 1000 m isobath contour on the International Bathymetric Chart of the Arctic Ocean [48]. To determine the percent areal coverage of aragonite undersaturation, the interpolated area of undersaturation (371,525 km^2) was divided by the area of the Canadian Basin (1,858,888 km^2).

Bacterial Production Rates

Bacterial production rates (*BP*; mg C m^{-3} d^{-1}) were calculated using the following relationship:

$$\mathrm{BP} = 0.39(\mathrm{Chl\text{-}a}) + 0.52(\mathrm{T}) + 0.11$$

where *Chl-a* is chlorophyll *a* (μg L^{-1} d^{-1}) and *T* is temperature (°C). This equation was derived from data previously collected in the Arctic Ocean during the same season as this study [49].

Statistical Analyses

An initial assessment of the complete data set indicated that waters were not homogenous throughout the sampled area. The data set was therefore sorted into four regions based on differences in salinity and other measured parameters (Table 1): the Beaufort Sea, Makarov Basin, Sever Spur, and Canada Basin regions. The sample sites for the HLY1102 data set extend to higher latitudes than the HLY1002 data set and were therefore used to conservatively delineate these geographic boundaries. Comparisons for significant differences or similarities between each region were performed using the f_{SIM}, f_{MW}, f_{SW}, Ω_a, pCO_2, *S*, *T*, *Chl-a*, and *BP* data sets. The data from each region were not normally distributed as determined by the Shapiro-Wilk normality test ($\alpha = 0.05$). Accordingly, comparisons of variables were performed using the nonparametric Kruskal-Wallis one-way ANOVA (KW ANOVA, $\alpha = 0.05$), followed by an all-pairwise multiple comparison of median values using Dunn's method ($\alpha = 0.05$). Dunn's method for multiple comparisons determines which of the comparisons analyzed by KW ANOVA are significantly different. A *p*-value of <0.05 indicates a significant difference between the two median values. The Spearman rank-order method was used for all correlation calculations.

Rates of change of Ω_a were obtained by comparing September 1997 data [50] to the *Healy* 2010 and 2011 data. Surface *TA* and TCO_2 from similar locations were used to calculate Ω_a as described above. Rate of change for a given location was then calculated as the slope of a linear fit of Ω_a vs. year. The 1997 TCO_2 and *TA* data were analyzed on board using Dickson Certified Reference Material for every 20 samples to evaluate accuracy. Precision for the 1997 data was ~0.1% for TCO_2 and ~0.2% for *TA*.

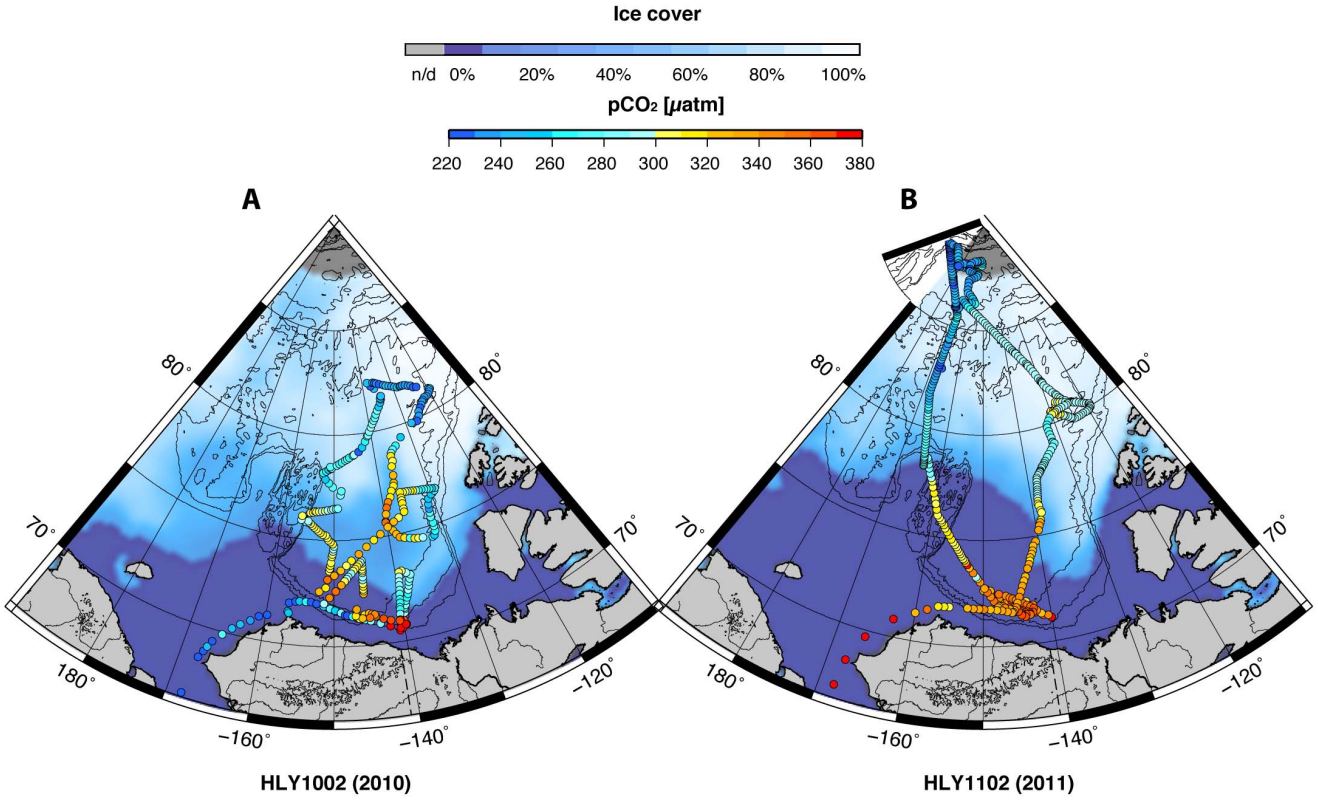

Figure 6. Surface pCO_2 in the western Arctic Ocean. (A) HLY1002. (B) HLY1102. The data points show underway pCO_2 values recorded at locations where discrete surface water samples were collected. The maps also show average sea ice concentration (% ice cover) for August 2010 and September 2011, respectively [70].
doi:10.1371/journal.pone.0073796.g006

Data Management

The data reported here are available at http://pubs.usgs.gov/ds/741/and http://pubs.usgs.gov/ds/748/.

Results

Spatial Coverage

In the course of the late-summer 2010 and 2011 *Healy* cruises, more than 34,000 water samples (flowthrough and discrete) were analyzed for *S*, *T*, pCO_2, *Chl-a*, and *BP*, and calculated Ω_a (Figure 1). The resulting data sets are among the most comprehensive in the region (Previous work in the area shown in Figure 1 had collectively produced ~19,900 data records). Sampling length intervals ranged from approximately 0.24 km to 10 km or more, depending on ship speed and sampling frequency. Table 2 shows median and range values for the HLY1102 data records that contain a complete suite of all of the following parameters: Ω_a, *S*, *T*, pCO_2, f_{SIM}, f_{MW}, f_{SW}, *Chl-a*, and *BP*.

Regionally Distinct Seawater Properties

The four delineated regions of the western Arctic (Table 2) are the Beaufort Sea, Canada Basin, Makarov Basin, and Sever Spur regions. Although these names coincide with geographic regions rather than oceanographic regimes, the Beaufort Sea is predominantly shallow and coastal, while the other regions are predominantly deep basins. In pairwise comparisons, the regions exhibit significant differences in four or more of the seawater variables of Ω_a, *S*, *T*, pCO_2, f_{SIM}, f_{MW}, f_{SW}, *Chl-a*, and *BP* (Table 3).

Figure 4 shows climatological August surface salinity through 1997 [52] and surface salinity encountered on the HLY1002 and HLY1102 cruises. The recent data show a generally lower *S* than is seen in the estimates of long-term means. The *Healy* data also show *S* increasing with increasing latitude (Figure 4) and ice cover (Figure 5). A concomitant increase in Ω_a with decreasing pCO_2 occurred along this same latitudinal trend (Figures 5 and 6). An exception to this general pattern is the Beaufort Sea region, which shows higher Ω_a values in the samples near the coast.

Aragonite Undersaturation and Water Mass Sources

Our calculations of Ω_a in the combined Canada and Makarov basins indicate that in the summers of 2010 and 2011, approximately 20% of the 1.9 million km^2 surface area was undersaturated with respect to aragonite (i.e., $\Omega_a<1$; Figure 5). All observed undersaturation was confined to the Canada Basin and Beaufort Sea. Undersaturated water extended poleward from the Beaufort Sea to nearly 80°N between the Canadian Archipelago and the Chukchi Cap (over 3.7×10^5 km^2). Waters supersaturated with respect to aragonite were seen in the Makarov Basin and Sever Spur areas ($1.14\leq\Omega_a\leq1.61$) in association with nearly 100% sea ice cover and relatively low pCO_2 (Figures 5 and 6). Pairwise statistical comparisons show that Ω_a values in these two regions were significantly greater than in the Canada Basin (Table 3). Beaufort Sea coastal waters had Ω_a values significantly lower than Makarov Basin waters.

Sea ice melt showed the greatest contribution to water masses in the Beaufort Sea and Canada Basin (f_{SIM} up to 0.219) and comparatively low contributions in the Makarov Basin and Sever

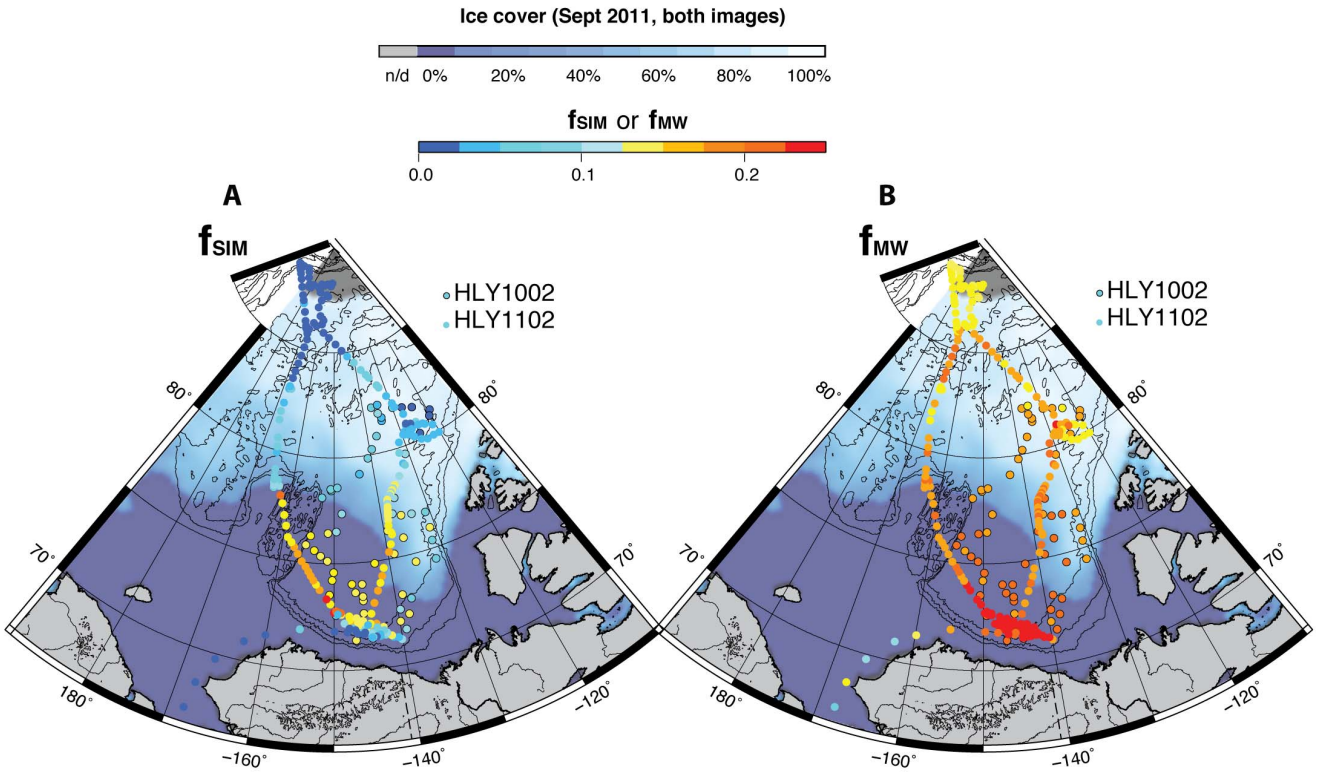

Figure 7. Modeled freshwater fractional contributions to surface waters of the western Arctic Ocean. (A) Fraction of sea ice melt, f_{SIM}. (B) Fraction of meteoric water, f_{MW}. The maps also show average sea ice concentration (% ice cover) during September 2011 [70].
doi:10.1371/journal.pone.0073796.g007

Spur areas (f_{SIM} up to 0.061; Table 1, Figure 7). Values of f_{MW} were more homogenous throughout the study area but were generally lower in the Makarov Basin and Sever Spur areas (0.116–0.177) than in the Beaufort Sea and Canada Basin (0.054–0.307).

Surface water Ω_a was strongly and positively correlated with surface S in all localities (Table 4). Further, S in all localities was strongly but negatively correlated with the fraction of fresh water derived from sea ice meltwater (f_{SIM}) and/or meteoric water (f_{MW}; Table 4). Values of f_{MW} showed a consistent negative correlation to Ω_a throughout the entire western Arctic, including waters in ice-covered areas such as the Makarov Basin.

Aragonite Undersaturation and Biological Processes

Aragonite saturation state can be influenced by not only air–sea CO_2 exchange but also biological activities such as carbon fixation and respiration. Photoautotrophic organisms may remove CO_2 from the water, thereby tending to increase Ω_a. Respiration, in contrast, adds CO_2, thereby tending to decrease Ω_a. During our late summer cruises, *Chl-a*, which is indicative of photoautotrophic activity, showed no significant correlation with Ω_a except in the Canada Basin (Table 4), where the correlation was positive. *Chl-a* and pCO_2 also positively covaried in the Canada Basin. The pCO_2: Ω_a relationship was significantly and negatively correlated in the Makarov Basin and showed no significant association in the other regions.

Discussion

Projections of the extent and rate of Arctic Ocean acidification and the associated ecosystem changes require models based on causal relationships and complex feedbacks among rapidly changing physical, chemical, and biological processes. Model formulation and validation both require extensive data sets. Our baseline study significantly expands the body of data available for such work and also provides the first high-resolution data from higher latitude waters (up to 88°48′ N into the Makarov Basin; Figure 1). Previous work has focused primarily on coastal areas of the southern Canada Basin and the Bering and Beaufort Seas [20,22,25,51–55]. The new data provide a basis for detecting future change and analyzing trends in surface water chemistry.

Combined with older data, the 2010–2011 measurements can also provide insight into changes that have already occurred in the Arctic, primarily over the past two decades. (Canadian Basin carbonate chemistry data from before the 2000s are sparse.) For example, a comparison with 1994 cruise data [50] indicates that surface S in the northern Canada Basin and the Makarov Basin (i.e., above ~80°N) decreased only slightly over the 17 intervening years, from 31.48 in 1994 ($n = 33$) to 30.61 in 2011 ($n = 49$). Over roughly the same time period, a large decrease in average S occurred in the Beaufort Sea–southern Canada Basin (~72–75°N), from 28.49 (late September 1997, $n = 19$; [50]) to 23.51 (September 2010, $n = 53$).

This marked surface freshening was accompanied by a large decrease in average Ω_a, from 1.31 to 1.14, which suggests a link between Ω_a and dilution from sea ice melt in these areas. A number of locations that were supersaturated with respect to aragonite in 1997 were undersaturated in 2010 and 2011. Based on the limited data available from sites in the southern Canada Basin, we estimate that summer surface Ω_a decreased at a rate of 2.1% yr^{-1} between 1997 and 2010–nearly an order of magnitude greater than the average rate observed for the Pacific Ocean (0.36% yr^{-1}; [56]).

Table 4. Spearman rank-order correlations between the Arctic Ocean regions.

Region	Parameter	f_{SIM}	f_{MW}	f_{SW}	T (°C)	*S*	pCO_2	*Chl-a* (mg m^{-3})	*BP* (mg C m^{-3} d^{-1})
Beaufort Sea (BS)	Ω_a	−0.908**	−0.370**	0.797**	*ns*	0.782**	*ns*	*ns*	*ns*
Makarov Basin (MB)		−0.370**	−0.791**	0.830**	−0.788**	0.849**	−0.827**	*ns*	0.563**
Sever Spur (SS)		*ns*	−0.843**	0.825**	−0.567**	0.849**	*ns*	*ns*	0.526**
Canada Basin (CB)		−0.866**	−0.517**	0.837**	0.349**	0.830**	*ns*	0.493**	0.504**
	BS	f_{SIM}	0.534**	−0.932**	*ns*	−0.920**	*ns*	−0.391**	*ns*
	MB		*ns*	−0.667**	0.323*	−0.620**	*ns*	*ns*	−0.343*
	SS		*ns*	−0.477*	0.410*	−0.410*	*ns*	*ns*	*ns*
	CB		0.542**	−0.945**	−0.336**	−0.935**	*ns*	−0.467**	−0.517**
		BS	f_{MW}	−0.804**	0.671**	−0.823**	*ns*	*ns*	0.670**
		MB		−0.759**	0.845**	−0.795**	0.562**	*ns*	−0.377*
		SS		−0.726**	0.540*	−0.775**	*ns*	*ns*	−0.517**
		CB		−0.786**	−0.500**	−0.804**	−0.453**	−0.531**	−0.582**
			BS	f_{SW}	−0.365*	0.999**	*ns*	0.363*	−0.358*
			MB		−0.840**	0.996**	−0.433*	*ns*	0.504**
			SS		−0.783**	0.997**	*ns*	0.511*	0.687**
			CB		0.441**	0.999**	0.198*	0.549**	0.606**
				BS	*T*	−0.384**	0.706**	*ns*	*ND*
				MB		−0.869**	0.496**	*ns*	*ND*
				SS		−0.778**	*ns*	−0.675**	*ND*
				CB		0.448**	0.663**	0.779**	*ND*
					BS	*S*	ns	0.358*	−0.378*
					MB		−0.464*	*ns*	0.495**
					SS		*ns*	0.501*	0.687**
					CB		0.212*	0.553**	0.611**
						BS	pCO_2	*ns*	0.709**
						MB		*ns*	−0.417*
						SS		*ns*	*ns*
						CB		0.389**	0.587**

A significant correlation between parameters is denoted by * at $p<0.05$ or by ** at $p<0.001$. An entry of *ns* indicates no significant correlation. An entry of *ND* indicates no data.

doi:10.1371/journal.pone.0073796.t004

Effects of Sea Ice Melt on Aragonite Saturation State

The observed decrease in aragonite mineral saturation state in the southern Canada Basin since 1997 has been accompanied by a decrease in late summer salinity (Figure 4). Increased freshwater in the Arctic Ocean is known to have diluted surface mixed layer *S* over the past decade [57–61]. This freshening may have been enhanced in the western Arctic, where recent spin-up of the wind-driven convergence of the Beaufort Gyre may have increased freshwater retention [57,60]. The strong vertical density gradient of the Arctic Ocean also acts to maintain low *S* in the surface mixed layer (~0–50 m depth) throughout the seasons [18]. The cold Arctic halocline at ~50–400 m depth reduces upward mixing of CO_2-rich deep waters to the surface mixed layer [18], thus playing a significant role in maintaining low surface *S* and Ω_a.

Comparisons of *S* and Ω_a show a significant correlation throughout the study area (Figures 4, 5, and 8; Table 4), suggesting that dilution with freshwater provides a direct mechanism for reducing saturation state [8,21]. The water-mass mixing model distinguishes the proportion of freshwater derived from sea ice melt (f_{SIM}) vs. meteoric water (f_{MW}; i.e., terrestrial runoff and direct precipitation). Relatively high f_{SIM} was observed in areas south of ~80°N (Figure 8A), notably in those areas where summer ice extent had recently decreased and particularly where multiyear ice had melted. The strong negative correlation between f_{SIM} and Ω_a in the Beaufort Sea and Canada Basin (Figure 8, Table 4) reflects the dominant influence predicted by dilution from sea ice meltwater on aragonite saturation state. Areas north of 80°N, such as the Makarov Basin and Sever Spur regions, were largely immune to the effects of sea ice melt on aragonite undersaturation, showing weak to no significant correlation between f_{SIM} and Ω_a.

The influence of f_{MW} (Figure 7B) was more homogenous than f_{SIM} (Figure 7A). Within the relatively narrow f_{MW} range encountered, highest values occurred in Beaufort Sea coastal waters while lower values occurred in the ice-covered Makarov Basin. Overall, f_{MW} values were negatively correlated to Ω_a in all regions, which reflects the spatially consistent role of meteoric freshwater in reducing Ω_a. Still, those correlations were relatively weak compared to the correlations between f_{SIM} and Ω_a in the Beaufort Sea and Canada Basin (Table 4), where Ω_a is strongly affected by sea ice meltwater.

The variable influence of freshwater sources across the regions is evident in the geographic distribution (clustering) of the data

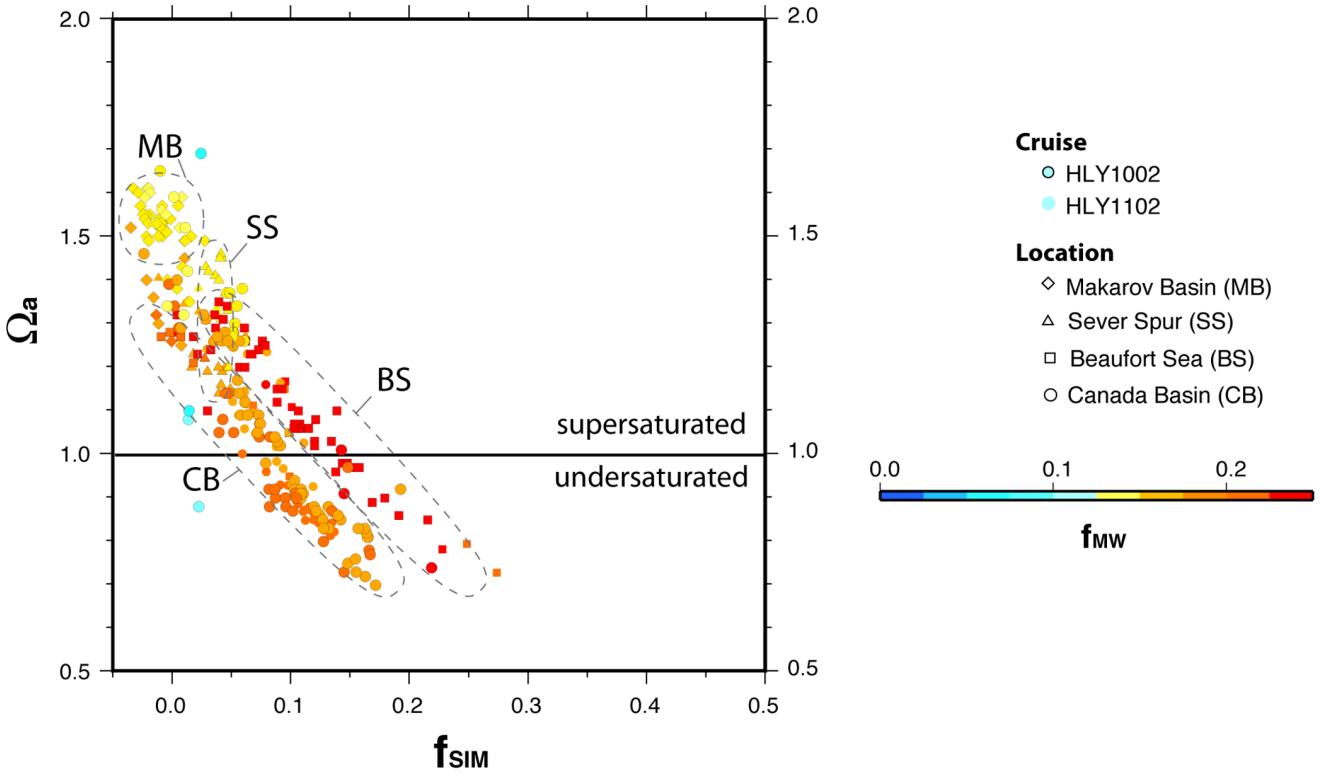

Figure 8. Aragonite saturation state and freshwater contributions in regions of the western Arctic Ocean. Comparison of aragonite saturation state (Ω_a) to freshwater source fractions (f_{SIM} plotted on *x*-axis, f_{MW} coded to point color). Symbol shapes identify the basin, where the data were collected. Ellipses outline general data clusters from each region.
doi:10.1371/journal.pone.0073796.g008

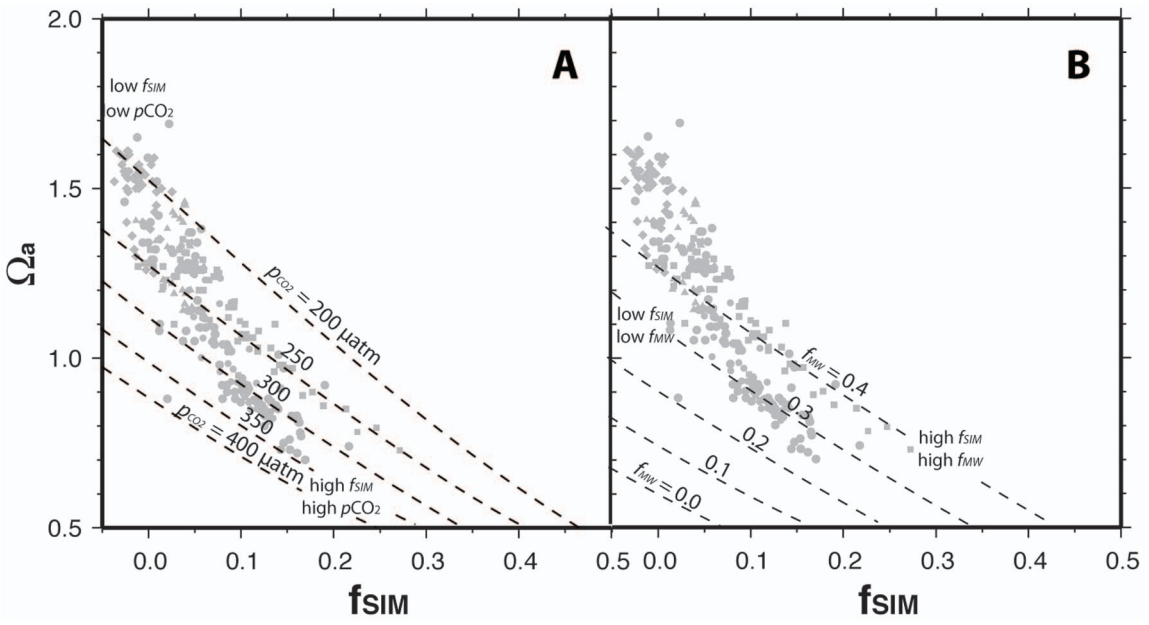

Figure 9. Modeled Ω_a:f_{SIM} for conservative mixing of seawater and sea ice meltwater. (A) Effect of variable pCO_2 with constant $f_{MW} = 0.18$. (B) Effect of variable f_{MW} with constant $pCO_2 = 372.6$ µatm. The values of the constants are equal to the mid-range values observed during the 2011 cruise. The gray points show the data from Figure 8. For the freshwater end-member [33,35,39,55], $TA_{MW} = 1000$ µmol kg^{-1}, $S_{FW} = 0$, and $TCO_{2MW} = 940$ µmol kg^{-1}. For the sea ice meltwater end-member [40,71], $TA_{SIM} = 540$ µmol kg^{-1}, $S_{SIM} = 4$, and $TCO_{2SIM} = 300$ µmol kg^{-1}. Atlantic seawater is characterized according to mean values observed at the thermocline in the HLY1102 station data, 250–400 m depth: $TA_{SW} = 2318.5$ µmol kg^{-1}, $S_{SW} = 34.92$, and $TCO_{2SW} = 2156.6$ µmol kg^{-1}). All models are calculated at a seawater *T* of −1.47°C (median value of the HLY1102 data set).
doi:10.1371/journal.pone.0073796.g009

shown in Figure 8. For the data set as a whole, Ω_a is negatively correlated with f_{SIM}, but regional distinctions are apparent. The Makarov Basin and Sever Spur areas are generally characterized by relatively supersaturated Ω_a values and generally low f_{SIM} (Tables 2, 4). The Canada Basin and Beaufort Sea data show a strong correlation between Ω_a and f_{SIM}, but for a given f_{SIM} value, Beaufort Sea Ω_a values are higher than those from the Canada Basin. This offset is likely due to the fact that meteoric water from river runoff, which is more abundant in the coastal waters of the Beaufort Sea (Figure 7B), contributes higher concentrations of dissolved calcium, inorganic carbon, and carbonate alkalinity than does sea ice melt [22]. As a result, Beaufort Sea surface waters are more strongly supersaturated than Canada Basin waters for an equivalent contribution of freshwater from sea ice melt. This effect, observed strongly in the Beaufort Sea, is likely enhanced by the fact that North American rivers carry more calcium, inorganic carbon, and carbonate alkalinity than do Eurasian rivers [39]. Thus, the net effect of meteoric water on lowering Ω_a values is likely less significant in the southern Canada Basin and Beaufort Sea, where the Mackenzie River is the primary meteoric water source, than in the Makarov Basin (Figure 7B), where Eurasian rivers are the primary source. Over the past decade, the Makarov Basin has received increased input from these rivers [59]. Differences between pelagic and coastal waters may also be partially attributed to a pronounced upwelling event that occurred in the Beaufort Sea during late summer 2011 [52]. This coastal upwelling may account for a reduced MW role, resulting in somewhat higher regional Ω_a values in 2011 than in 2010.

Regarding the relative roles of f_{MW} and f_{SIM}, it is worth noting that our sensitivity analysis (Figure 2) suggests that f_{MW} values may in some cases be overestimated due to the simplifying assumption that the SW end-member is Atlantic-derived. A portion of the freshwater attributed in our analysis to terrestrial runoff from Arctic rivers may in actuality derive from Bering Strait Inflow. However, the inference of a strong regional relationship between sea ice melt and low Ω_a remains robust, being relatively insensitive to model assumptions.

The observed negative correlation between f_{SIM} and Ω_a (Figure 8) may convolve the two hypothesized effects of reduction of sea ice cover on Ω_a–namely, dilution with meltwater and exposure to the CO_2-rich atmosphere, both of which may act to reduce Ω_a in areas of recent sea ice melt. Figure 9A illustrates the combined roles of these two effects in a simple model of conservative mixing between end-member seawater and sea ice meltwater. Model lines show variation of the f_{SIM}: Ω_a relationship under conditions in which pCO_2 is varied while f_{MW} is held constant (dashed lines show model curves; gray points show observed data). The model lines show that for a given f_{SIM} contribution, a higher pCO_2 corresponds to a lower saturation state. As predicted by the model, Ω_a is negatively correlated with f_{SIM}, but the slope for the correlation of the observed data is steeper than model predictions. The greater slope associated with the observations is likely due to the combination of the two sea-ice–related effects on Ω_a. For instance, waters represented by points at the left side of the data cluster derive predominantly from the Makarov Basin, where Ω_a is generally highest. These waters show low f_{SIM} values, due to minimal melting of sea ice, and also low pCO_2 values, reflecting disequilibrium with the atmosphere (labeled "low f_{SIM}, low pCO_2" in Figure 9A). In contrast, waters in areas of recent sea ice melt, such as the Canada Basin or Beaufort Sea, show high f_{SIM} values and generally high pCO_2 (labeled "high f_{SIM}, high pCO_2" in Figure 9A). The combination of the disequilibrium effect with the meltwater effect tends to produce a trend connecting the data from these two regions, with a steeper slope than is predicted by a model that includes seawater–meltwater mixing only.

Figure 9B shows a similar model of conservative mixing of seawater and sea ice meltwater, but in this case varying f_{MW} while holding pCO_2 constant. Again, the model lines show that a higher fractional contribution of sea ice melt corresponds to a lower saturation state. However, the addition of meteoric water tends to partially counter the effect of SIM: for a given meltwater contribution (f_{SIM}), increasing the meteoric contribution (f_{MW}) corresponds to a higher saturation state. As with Figure 9A, the observed data show a steeper negative slope than that predicted by the simple two-component mixing model. However, f_{SIM} and f_{MW} are observed to be positively correlated throughout the Canada Basin and Beaufort Sea (Table 4). Connecting regions of "low f_{SIM}, low f_{MW}" and "high f_{SIM}, high f_{MW}" in Figure 9B suggests that the correlation between these variables would tend to counter the "steeper-than-predicted" slope of the correlation between f_{SIM} and Ω_a discussed above.

The model shown in Figure 9B also illustrates the proposed explanation for the positive offset of Ω_a values (for a given f_{SIM}) from the Beaufort Sea as compared to the Canada Basin (Figure 8). Model calculations of the f_{SIM}: Ω_a relationship are offset to higher Ω_a values as a result of high modeled f_{MW}. This effect is seen predominantly in the Beaufort Sea. This effect is likely due to terrestrial contributions of dissolved calcium, inorganic carbon, and carbonate alkalinity from the Mackenzie River [39].

Effects of Biological Activity on Aragonite Saturation State

Variation in Ω_a and pCO_2 values show the effects of not only hydrodynamic forcing [24], regional sea ice melt, and terrestrial inputs of freshwater and CO_2 [25], but also local biological processes. Consistent with previous Arctic Ocean surface water observations [62], our Makarov Basin measurements showed low CO_2 partial pressures compared to atmospheric values. Seawater pCO_2 ranged from 242 to 330 μatm; atmospheric values at the time were ~380 μatm or higher. Seawater pCO_2 values lower than atmospheric values have previously been attributed to (a) incomplete seawater equilibration with the present-day atmosphere and (b) cooling [8,17,20], but also (c) relatively low net community production in areas of offshore basins as compared to coastal waters [8].

Bacterial metabolism is the collective process of bacterial production (*BP*) (Table 2) and respiration (*BR*). Bacterial production pathways produce biomass, while respiration pathways generate energy for cellular processes. The *BR* reactions release CO_2 when organic and inorganic C are substrates. The efficiency at which bacteria incorporate C into their biomass is a fraction of the total C utilized by the heterotrophic microbial community. This efficiency is described by the bacterial growth efficiency [$BGE = BP/(BP+BR)$] [63]. In general, BGE values range from 0.03 to 0.27 in open marine waters and from 0.09 to 0.45 in coastal waters. *BGE* values in the western Arctic Ocean have been shown to be relatively low, averaging only 0.07 ± 0.09 [49,64]. The low BGE indicates that a significant proportion of the utilized C is being used in respiration-related processes, which produce and release CO_2.

Differences in the *BGE* of heterotrophic microbial communities in the four regions may explain the inconsistent correlations between pCO_2 and *BP*. These quantities are positively correlated in the Beaufort Sea and Canada Basin regions but are negatively correlated in the Makarov Basin and Sever Spur regions (Table 4). A confounding influence on these inconsistent correlations may be the overwhelming contribution of atmospheric pCO_2 exchange

relative to the heterotrophic microbial community production of pCO_2. The influence of heterotrophic microbial community respiration on pCO_2 and thereby Ω_a would be detected only if the effects (i.e., increasing pCO_2 and decreasing Ω_a) were greater than the net effect of CO_2 influences from the atmosphere, photoautotrophic communities, and freshwater additions.

Seasonal Trends

Seasonal trends of Ω_a in the Arctic Ocean are generally poorly documented (for an exception see [65]). Winter data collected in 2011 and 2012 between ~83°N and 87°N [62] provide, in combination with our Makarov Basin data, a rare opportunity for a seasonal comparison. In general, the winter and summer values of surface water Ω_a and pCO_2 were comparable. In addition, Makarov Basin under-ice mixed layer water (15–40 m below the ice) was sampled in April 2012 along a transect of the Switchyard Program (data archived by the Advanced Cooperative Arctic Data Information Service, aoncadis.org). The under-ice winter water was characterized by $T = -1.69 \pm 0.04$°C, $S = 31.0 \pm 0.7$, $pCO_2 = 312 \pm 13$ µatm, and $\Omega_a = 1.31 \pm 0.06$. These data are consistent with our Makarov Basin summer data (Table 2), indicating little seasonal variation in the surface water chemistry of the Makarov Basin.

Implications for Modeling of Future Chemical Changes

Models have projected that large areas of the Arctic Ocean will become undersaturated with respect to aragonite in the next decade [3–6]. The data presented here indicate that the area of undersaturation presently extends to approximately 20% of the Canadian Basin in the late summer months, when sea ice is near its minimum extent. A number of other studies have shown areas of aragonite undersaturation in the Canadian Archipelago and on the Beaufort Sea shelf [21,23,24].

Projection of future freshening and undersaturation in areas currently under perennial ice cover, such as the Makarov Basin, may be facilitated by water source identification based on the use of salinity and oxygen isotopic composition as conservative tracers (e.g., Figures 7–9). Our analysis provides insight into how sea ice meltwater and meteoric water influence aragonite saturation states. The negative correlation between Ω_a and f_{SIM} (Figure 8, Table 4) characterizes the dependence of saturation state on the melting of multiyear sea ice and suggests a pattern along a transect from the Beaufort Sea to the Makarov Basin. The Makarov Basin represents an end-member whose chemical composition is essentially free of the effects of reduced sea ice cover and input of additional freshwater from melting of multiyear ice, while the southern Canada Basin represents conditions resulting from reduced sea ice. Given that summer ice-free conditions are projected to expand in the near term [10–12], these spatial trends allow prediction of the conditions under which the carbonate chemistry of the Makarov Basin will resemble that of the southern Canada Basin. Predictive models of ocean acidification must account for not only the effects of equilibration with atmospheric CO_2 but also freshwater dilution and biogeochemical processes.

Data from this study also suggest that an assumption of metabolic coupling or co-dependence between heterotrophic and photoautotrophic organisms in the Arctic Ocean is not appropriate for inclusion in predictive models of ocean acidification processes. Recent studies of the relation between bacterial production and primary production in coastal and pelagic Arctic waters have shown that these carbon cycling processes can proceed uncoupled [49,66,67]. These studies found that the degree of correlation depends on time of year, percentage of ice cover, hydrodynamic regime, bacterial abundance, and bacterial growth efficiency. The absence of predictable correlations between biological variables and Ω_a in this study indicate that complex interactions are driving the biogeochemical processes. Uncoupling of these processes and variability in their rates and efficiencies have important implications for not only the retention of C at shallower productive depths [68] but also for the formulation of models that predict the influence of heterotrophic and photoautotrophic processes on pCO_2.

In conclusion, the data presented here collectively suggest that recent decreases in western Arctic Ocean Ω_a can be predominantly attributed to recent melting of multiyear sea ice and the associated seawater freshening and uptake of atmospheric CO_2; biogeochemical processes exert an additional influence. Despite increasing awareness of rapid global change in the Arctic, much remains to be done with respect to predicting changes in marine surface water chemistry. For example, few data are available for the polar winter, and it is not known whether aragonite-undersaturated areas decrease in size with the seasonal freezing of sea ice. Also, while the effects of sea ice melt may diminish over the long term, the effects of increasing terrestrial runoff and direct precipitation are likely to persist [69]. Quantitative documentation of these processes in the Arctic Ocean is needed for refinement of the next generation of global ocean acidification models.

Acknowledgments

We thank the captains and crew of the HLY1002 and HLY1102 cruises. We also thank Brian Edwards, Chief Scientist on HLY1002, and Larry Mayer and Andy Armstrong, Co-Chief Scientists on HLY1102, for their support of this non-interference science during the U.S. Extended Continental Shelf Task Force cruises. S. Roberts and D. Chayes provided shipboard technical help. T. Newberger constructed and maintained the Lamont-Doherty pCO_2 system. B. Buczkowski, C. Dufore, B. Moore, M. Hansen, C. Puscas, and N. Smiley helped with cruise preparation and data collection and processing during and after the cruises. T. Clayton, as well as two anonymous reviewers, provided helpful comments on this manuscript.

Author Contributions

Conceived and designed the experiments: LLR JGW JTL KKY. Performed the experiments: LLR JGW KKY JTL POK XL MCP RHB KAS TT. Analyzed the data: LLR JGW JTL KKY POK XL RHB KAS TT. Contributed reagents/materials/analysis tools: LLR JGW RHB TT KKY. Wrote the paper: LLR JGW JTL KKY RHB KAS TT.

References

1. National Research Council (2010) Ocean acidification: A national strategy to meet the challenges of a changing ocean. Washington, D.C.: National Academies Press. 175 p.
2. Caldeira K, Wickett ME (2003) Anthropogenic carbon and ocean *p*H. Nature 425: 365.
3. Orr JC, Fabry VJ, Aumont O, Bopp L, Doney SC, et al. (2005) Anthropogenic ocean acidification over the twenty-first century and its impact on calcifying organisms. Nature 437: 681–686.
4. Popova EE, Yool A, Coward AC, Anderson TR (2013) Regional variability of acidification in the Arctic: A sea of contrasts. Biogeosciences Discuss 10: 2937–2965.
5. Steinacher M, Joos F, Frolicher TL, Plattner GK, Doney SC (2009) Imminent ocean acidification in the Arctic projected with the NCAR global coupled carbon cycle-climate model. Biogeosciences 6: 515–533.
6. Yamamoto A, Kawamiya M, Ishida A, Yamanaka Y, Watanabe S (2012) Impact of rapid sea-ice reduction in the Arctic Ocean on the rate of ocean acidification. Biogeosciences 9: 2365–2375.

7. Fabry VJ, McClintock JB, Mathis JT, Grebmeier JM (2009) Ocean acidification at high latitudes: The bellweather. Oceanography 22: 160–171.
8. Bates NR, Mathis JT (2009) The Arctic Ocean marine carbon cycle: Calculation of air–sea CO_2 exchanges, ocean acidification impacts and potential feedbacks. Biogeosciences 6: 2433–2459.
9. Parmentier F-JW, Christensen TR, Sørensen LL, Rysgaard S, McGuire AD, et al. (2013) The impact of low sea-ice extent on Arctic greenhouse-gas exchange. Nat Clim Change 3: 195–203.
10. Maslanik J, Stroeve JC, Fowler C, Emery W (2011) Distribution and trends in Arctic sea ice age through spring 2011. Geophys Res Lett 38: L13502, doi: http://dx.doi.org/10.1029/2011GL047735.
11. Perovich DK, Richter-Menge JA, Jones KF, Light B (2008) Sunlight, water, and ice: Extreme Arctic sea ice melt during the summer of 2007. Geophys Res Lett 35: L11501, doi: http://dx.doi.org/10.1029/2008GL034007.
12. Stroeve JC, Maslanik J, Serreze MC, Rigor I, Meier W, et al. (2011) Sea ice response to an extreme negative phase of the Arctic Oscillation during winter 2009/2010. Geophys Res Lett 38: L02502, doi: http://dx.doi.org/10.1029/2010GL045662.
13. Polyakov IV, Timokhov LA, Alexeev VA, Bacon S, Dmitrenko IA, et al. (2010) Arctic Ocean warming contributes to reduced polar ice cap. J Phys Oceanogr 40: 2743–2756.
14. Zhang J, Lindsay R, Schweiger A, Steele M (2013) The impact of an intense summer cyclone on 2012 Arctic sea ice retreat. Geophys Res Lett 40: 720–726.
15. Bates NR, Moran SB, Hansell DA, Mathis JT (2006) An increasing CO_2 sink in the Arctic Ocean due to sea-ice loss. Geophys Res Lett 33: L23609, doi: http://dx.doi.org/10.1029/2006GL027028.
16. Cai W-J, Chen L, Chen B, Gao Z, Lee SH, et al. (2010) Decrease in the CO_2 uptake capacity in an ice-free Arctic Ocean basin. Science 329: 556–559.
17. Jutterström S, Anderson LG (2010) Uptake of CO_2 by the Arctic Ocean in a changing climate. Mar Chem 122: 96–104.
18. Martinson DG, Steele M (2001) Future of the Arctic sea ice cover: Implications of an Antarctic analog. Geophys Res Lett 28: 307–331.
19. Takahashi T, Sweeney C, Hales B, Chipman DW, Newberger T, et al. (2012) The changing carbon cycle in the Southern Ocean. Oceanography 25: 26–37.
20. Bates NR, Cai W-J, Mathis JT (2011) The ocean carbon cycle in the western Arctic Ocean: Distributions and air–sea fluxes of carbon dioxide. Oceanography 24: 186–201.
21. Yamamoto-Kawai M, McLaughlin FA, Carmack EC, Nishino S, Shimida K (2009) Aragonite undersaturation in the Arctic Ocean: Effects of ocean acidification and sea ice melt. Science 326: 1098–1100.
22. Azetsu-Scott K, Clarke A, Falkner K, Hamilton J, Jones EP, et al. (2010) Calcium carbonate saturation states in the waters of the Canadian Arctic Archipelago and the Labrador Sea. J Geophys Res Oceans 115: C11021, doi: http://dx.doi.org/10.1029/2009JC005917.
23. Bates NR, Mathis JT, Cooper LW (2009) Ocean acidification and biologically induced seasonality of carbonate mineral saturation states in the western Arctic Ocean. J Geophys Res 114: C11007, doi: http://dx.doi.org/10.1029/2008JC004862.
24. Chierici M, Fransson A (2009) Calcium carbonate saturation in the surface water of the Arctic Ocean: Undersaturation in freshwater-influenced shelves. Biogeosciences 6: 2421–2432.
25. Mathis JT, Cross JN, Bates NR (2011) Coupling primary production and terrestrial runoff to ocean acidification and carbonate mineral suppression in the eastern Bering Sea. J Geophys Res 116: C02030, doi: http://dx.doi.org/10.1029/2010JC006453.
26. Jutterström S, Anderson LG (2005) The saturation of calcite and aragonite in the Arctic Ocean. Mar Chem 94: 101–110.
27. Chayes D, Roberts S, Bolmer T (2010) HLY1002 data description summary. Unpublished report of the HLY1002 cruise.
28. Wang ZA, Liu X, Byrne RH, Wanninkhof R, Bernstein RE, et al. (2007) Simultaneous spectrophotometric flow-through measurements of *p*H, carbon dioxide fugacity, and total inorganic carbon in seawater. Anal Chim Acta 596: 23–36.
29. Dickson AG, Sabine CL, Christian JR, editors (2007) Guide to best practices for ocean CO_2 measurements. PICES Special Publication 3. 191 p.
30. Liu X, Patsavas MC, Byrne RH (2011) Purification and characterization of meta-cresol purple for spectrophotometric seawater *p*H measurements. Environ Sci Technol 45: 4862–4868.
31. Craig H, Gordon LI (1965) Deuterium and oxygen-18 variations in the ocean and marine atmosphere. In: Tongiogi E, editor, Proceedings of a conference on stable isotopes in oceanographic studies and paleotemperatures. Spoleto, Italy: Laboratorio di Geologia Nucleare, Pisa, Italy. 9–130.
32. Bauch D, Erlenkeuser H, Andersen N (2005) Water mass processes on Arctic shelves as revealed from $\delta^{18}O$ of H_2O. Glob Planet Change 48: 165–174.
33. Bauch D, Hölemann J, Dmitrenko IA, Janout MA, Nikulina A, et al. (2012) The impact of Siberian coastal polynyas on shelf-derived Arctic Ocean halocline waters. J Geophys Res 117: C00G12, doi: http://dx.doi.org/10.1029/2011JC007282.
34. Bauch D, Schlosser P, Fairbanks RG (1995) Freshwater balance and the sources of deep and bottom waters in the Arctic Ocean inferred from the distribution of $H_2{}^{18}O$. Prog Oceanogr 35: 53–80.
35. Cooper LW, Benner R, McClelland JW, Peterson BJ, Holmes RM, et al. (2005) Linkages among runoff, dissolved organic carbon, and the stable oxygen isotope composition of seawater and other water mass indicators in the Arctic Ocean. J Geophys Res 110: G02013, doi: http://dx.doi.org/10.1029/2005JG000031.
36. Östlund HG, Hut G (1984) Arctic Ocean water mass balance from isotope data. J Geophys Res 89: 6373–6381.
37. Tan FC, Strain PM (1980) The distribution of sea ice meltwater in the eastern Canadian Arctic. J Geophys Res 85: 1925–1932.
38. Yamamoto-Kawai M, McLaughlin FA, Carmack EC, Nishino S, Shimada K, et al. (2009) Surface freshening of the Canada Basin, 2003–2007: River runoff versus sea ice meltwater. J Geophys Res 114: C00A05, doi: http://dx.doi.org/10.1029/2008JC005000.
39. Cooper LW, McClelland JW, Holmes RM, Raymond PA, Gibson JJ, et al. (2008) Flow-weighted values of runoff tracers ($\delta^{18}O$, DOC, Ba, alkalinity) from the six largest Arctic rivers. Geophys Res Lett 35: L18606, doi: http://dx.doi.org/10.1029/2008GL035007.
40. Pfirman S, Haxby W, Eicken H, Jeffries M, Bauch D (2004) Drifting Arctic sea ice archives changes in ocean surface conditions. Geophys Res Lett 31: L19401, doi: http://dx.doi.org/10.1029/2004GL020666.
41. Melling H, Moore RM (1995) Modification of the halocline source waters during freezing on the Beaufort Sea shelf: Evidence from oxygen isotopes and dissolved nutrients. Cont Shelf Res 15: 81–113.
42. Azetsu-Scott K, Petrie B, Yeats P, Lee C (2012) Composition and fluxes of freshwater through Davis Strait using multiple chemical tracers. J Geophys Res 117: C12011, doi: http://dx.doi.org/10.1029/2012JC008172.
43. Robbins LL, Hansen ME, Kleypas JA, Meylan SC (2010) CO2calc: A user-friendly seawater carbon calculator for Windows, Max OS X, and iOS (iPhone). U.S. Geological Survey Open-File Report 2010–1280. 17 p.
44. Lueker TJ, Dickson AG, Keeling CD (2000) Ocean pCO_2 calculated from dissolved inorganic carbon, alkalinity, and equations from K_1 and K_2: Validation based on laboratory measurements of CO_2 in gas and seawater at equilibrium. Mar Chem 70: 105–119.
45. Dickson AG (1990) Standard potential of the reaction: $AgCl(s) + 1/2H_2(g) = Ag(s) + HCl(aq)$, and the standard acidity constant of the ion HSO_4^- in synthetic sea water from 273.15 to 318.15 K. J Chem Thermodyn 22: 113–127.
46. Lee K, Kim T-W, Byrne RH, Millero FJ, Feely RA, et al. (2010) The universal ratio of boron to chlorinity for the North Pacific and North Atlantic oceans. Geochim Cosmochim Acta 74: 1801–1811.
47. Mucci A (1983) The solubility of calcite and aragonite in seawater at various salinities, temperature, and one atmosphere total pressure. Am J Sci 283: 780–799.
48. Jakobsson M, Macnab R, Mayer L, Anderson R, Edwards M, et al. (2008) An improved bathymetric portrayal of the Arctic Ocean: Implications for ocean modeling and geological, geophysical and oceanographic analyses. Geophys Res Lett 35: L07602, doi: http://dx.doi.org/10.1029/2008GL033520.
49. Garneau M, Roby S, Lovejoy C, Gratton Y, Vincent W (2008) Seasonal dynamics of bacterial biomass and production in a coastal arctic ecosystem: Franklin Bay, western Canadian Arctic. J Geophys Res 113: C07S91, doi: http://dx.doi.org/10.1029/2007JC004281.
50. Jones P, Azetsu-Scott K, Falkner K, McLaughlin F (2010) L.S. St-Laurent 18SNA097(Expocode: 18SN19970803), JOIS 97, Leg 1 cruise data from the 1997 cruises, CARINA Data Set. Carbon Dioxide Information Analysis Center, Oak Ridge National Laboratory, U.S. Department of Energy, Oak Ridge, Tennessee. Available: http://cdiac.ornl.gov/ftp/oceans/CARINA/L.S.St.Laurent/18SNA097/Leg1. Accessed 2013 Jun 13.
51. Antonov JI, Levitus S, Boyer TP, Conkright ME, O'Brien TD, et al. (1998) World Ocean Atlas 1998. NODC_WOA98 data provided by the NOAA Earth System Research Laboratory, Physical Sciences Division. Available: http://www.esrl.noaa.gov/psd/data/gridded/data.nodc.woa98.html. Accessed 2013 Jun 13.
52. Bates NR, Orchowska M, Garley R, Mathis JT (2012) Seasonal calcium carbonate undersaturation in shelf waters of the Western Arctic Ocean: How biological processes exacerbate the impact of ocean acidification. Biogeosciences Discuss 9,14255–14290.
53. Mathis JT (2011) The extent and controls on ocean acidification in the western Arctic Ocean and adjacent continental shelf seas: Arctic Report Card, Update for 2011, Available: http://www.arctic.noaa.gov/report11/ArcticReportCard_full_report.pdf.Accessed 2013 Jun 13.
54. Mathis JT, Pickart RS, Byrne RH, McNeil CL, Moore GWK, et al. (2012) Storm-induced upwelling of high pCO_2 waters onto the continental shelf of the western Arctic Ocean and implications for carbonate mineral saturation states. Geophys Res Lett 39: L07606, doi: http://dx.doi.org/10.1029/2012GL051574.
55. Yamamoto-Kawai M, McLaughlin FA, Carmack EC (2011) Effects of ocean acidification, warming and melting of sea ice on aragonite saturation of the Canada Basin surface water. Geophys Res Lett 38: L03601, doi: http://dx.doi.org/10.1029/2010GL045501.
56. Feely RA, Sabine CL, Byrne RH, Millero FJ, Dickson AG, et al. (2012) Decadal changes in the aragonite and calcite saturation state of the Pacific Ocean. Global Biogeochem Cycles 26: GB3001, doi: http://dx.doi.org/10.1029/2011GB004157.
57. Giles KA, Laxon SW, RIdout AL, Wingham DJ, Bacon S (2012) Western Arctic Ocean freshwater storage increased by wind-driven spin-up of the Beaufort Gyre. Nat Geosci 5: 194–197.

58. McPhee MG, Proshutinsky A, Morison JH, Steele M, Alkire MB (2009) Rapid change in freshwater content of the Arctic Ocean. Geophys Res Lett 36: L10602, doi: http://dx.doi.org/10.1029/2009GL037525.
59. Morison JH, Kwok R, Peralta-Ferriz C, Alkire MB, Rigor I, et al. (2012) Changing Arctic Ocean freshwater pathways. Nature 481: 66–70.
60. Rabe B, Karcher M, Schauer U, Toole JM, Krishfield RA, et al. (2011) An assessment of Arctic Ocean freshwater content changes from the 1990s to the 2006–2008 period. Deep Sea Res Part I Oceanogr Res Pap 58: 173–185.
61. Yamamoto–Kawai M, McLaughlin FA, Carmack EC, Nishino S, Shimada K (2008) Freshwater budget of the Canada Basin, Arctic Ocean, from salinity, $\delta^{18}O$ and nutrients. J Geophys Res 113: C01007, doi: http://dx.doi.org/10.1029/2006JC003858.
62. Takahashi T, Sutherland SC, Kozyr A (2012) Global ocean surface water partial pressure of CO_2 database: Measurements performed during 1957–2011 (version 2011). ORNL/CDIAC–160, NDP–088(V2011). Carbon Dioxide Information Analysis Center, Oak Ridge National Laboratory, U.S. Department of Energy, Oak Ridge., doi: http://dx.doi.org/10.3334/CDIAC/OTG.NDP088(V2011).
63. del Giorgio P, Cole J (1998) Bacterial growth efficiency in natural aquatic systems. Ann Rev Ecol Syst 29: 503–541.
64. Kirchman DL, Moran XA, Ducklow H (2009) Microbial growth in the polar oceans: Role of temperature and potential impact of climate change. Nat Rev Microbiol 7: 451–459.
65. Chierici M, Fransson A, Lansard B, Miller LA, Mucci A, et al. (2011) Impact of biogeochemical processes and environmental factors on the calcium carbonate saturation state in the Circumpolar Flaw Lead in the Amundsen Gulf, Arctic Ocean. J Geophys Res 116: C00G09, doi: http://dx.doi.org/10.1029/2011JC007184.
66. Jiao N, Herndl GJ, Hansell D, editors (2010) Microbial carbon pump in the ocean. Washington, D.C.: American Association for the Advancement of Science. 68 p.
67. Kirchman D, Hill V, Cottrell M, Gradinger R, Malmstrom R, et al. (2009) Standing stocks, production, and respiration of phytoplankton and heterotrophic bacteria in the western Arctic Ocean. Deep Sea Research Part II: Topical Stud Oceanogr 56: 1237–1248.
68. Nguyen D, Maranger R, Tremblay J, Gosselin M (2012) Respiration and bacterial carbon dynamics in the Amundsen Gulf, western Canadian Arctic. J Geophys Res 117: 1–12, doi: http://dx.doi.org/10.1029/2011JC007343.
69. Peterson BJ, Holmes RM, McClelland JW, Vörosmarty CJ, Lammers RB, et al. (2002) Increasing river discharge to the Arctic Ocean. Science 298: 2171–2173.
70. Fetterer F, Knowles K, Meier W, Savoie M (2009, updated) Sea Ice Index. Boulder: National Snow and Ice Data Center. Available: http://dx.doi.org/10.7265/N5QJ7F7W. Accessed: 2013 Jun 13.
71. Rysgaard S, Bendtsen J, Delille B, Dieckmann GS, Glud RN, et al. (2011) Sea-ice contribution to the air–sea CO_2 exchange in the Arctic and Southern Oceans. Tellus 63B: 823–830.